Offset-Free Direct Power Control of DFIG Under Continuous-Time Model Predictive Control

Rachid Errouissi, *Member, IEEE*, Ahmed Al-Durra, *Senior Member, IEEE*, S. M. Muyeen, *Senior Member, IEEE*, Siyu Leng, *Member, IEEE*, and Frede Blaabjerg, *Fellow, IEEE*

***Abstract*—This paper presents a robust continuous-time model predictive direct power control for doubly fed induction generator (DFIG). The proposed approach uses Taylor series expansion to predict the stator current in the synchronous reference frame over a finite time horizon. The predicted stator current is directly used to compute the required rotor voltage in order to minimize the difference between the actual stator currents and their references over the predictive time. However, as the proposed strategy is sensitive to parameter variations and external disturbances, a disturbance observer is embedded into the control loop to remove the steady-state error of the stator current. It turns out that the steady-state and the transient performances can be identified by simple design parameters. In this paper, the reference of the stator current is directly calculated from the desired stator active and reactive powers without encompassing the parameters of the machine itself. Hence, no extra power control loop is required in the control structure to ensure smooth operation of the DFIG. The feasibility of the proposed strategy is verified by the experimental results of the grid-connected DFIG and satisfactory performances are obtained.**

***Index Terms*—Continuous-time model predictive control (CTMPC), direct power control (DPC), disturbance observer, doubly fed induction generator (DFIG), renewable energy.**

I. Introduction

In the last few years, wind energy has been identified as the major contributor among all renewable energy resources, which has resulted in a strong increase wind power penetration into the electricity supply network. Wind energy conversion system (WECS) employs different type of electrical machines to produce electricity with zero emission. Among them, the doubly fed induction generator (DFIG) has been gradually occupying a larger market share due to several advantages, including variable speed operation, full power control capacity, high efficiency, low system cost, and decoupled active and reactive power control. Generally, the DFIG-based wind energy conversion technology uses back-to-back power electronic converters consisting of the rotor-side converter (RSC) and the grid-side converter (GSC) [1]. The control of the RSC and GRC allows both supersynchronous and subsynchronous operations. Typically, the rating of the back-to-back converter is around 30% of the generator capacity, resulting in cost savings compared to the full-scale converter. Taking into account the limited voltage of the back-to-back converter, the mechanical speed variation is about $\pm 30\%$ of the synchronous speed.

Traditionally, the DFIG is controlled using three approaches, namely, vector control (VC), direct torque control (DTC), and direct power control (DPC). The VC scheme [2] is widely used because of its design simplicity and it is formulated based on either stator voltage or flux orientation. As a result, the rotor current is decomposed into active and reactive power components in the synchronously rotating reference frame. Thus, the stator active and reactive powers can be independently controlled by regulating the rotor current components. Various rotor current controllers have been proposed, e.g., proportional-integral (PI) controller [3], [4], predictive control [5], sliding mode controller [6], etc. Generally, all the aforementioned methods offer a good performance in terms of robustness and disturbance rejection. However, the main drawback of the VC scheme is that the rotor current references highly rely on the machine parameters and stator flux. Such limitation implies the need for additional control loops to generate the rotor current references [2], [7].

The DTC was first introduced in [8] for controlling the squirrel-cage induction motor. The main idea of DTC is to instantaneously control the torque and the stator flux based on a predetermined voltage vector lookup table. Such a strategy necessitates the knowledge of the stator flux in magnitude and angle, as well as the electrical torque. For DFIG, as the stator windings are directly connected to the grid, the stator flux is constant in magnitude and frequency; hence, the DTC can be applied by regulating the rotor flux instead of the stator flux [9]. The DTC approach has several advantages, including fast transient response and low parameter dependence. Nonetheless, its implementation requires a high sampling frequency and leads to high and variable switching frequency, which may magnify the current ripples. In an attempt to overcome such a drawback, the hysteresis band, usually used in a DTC scheme, can be replaced by a simple torque controller [10]. On the other hand, space vector pulse width modulation can also be combined with the DTC approach to solve the problem of variable switching frequency [11]. With these improvements in DTC, good dynamic performance can be achieved; however, for power regulation, an external loop is still required to ensure good steady-state performance.

An alternative way to tackle the need for an extra loop is to use a control scheme that directly generates the rotor voltage

Manuscript received December 19, 2015; revised March 19, 2016; accepted April 19, 2016. Date of publication April 25, 2016; date of current version December 9, 2016. This work was supported by The Petroleum Institute Research Center Research Grant. Recommended for publication by Associate Editor V. Staudt. *(Corresponding author: Dr. S. M. Muyeen.)*

R. Errouissi, A. Al-Durra, S. M. Muyeen, and S. Leng are with the Petroleum Institute, Abu Dhabi 2533, UAE (e-mail: rerrouissi@pi.ac.ae; aldurra@pi.ac.ae; smmuyeen@pi.ac.ae; sleng@pi.ac.ae).

F. Blaabjerg is with the Department of Energy Technology, Faculty of Engineering and Science, Aalborg University, Aalborg 9220, Denmark (e-mail: fbl@et.aau.dk).

Color versions of one or more of the figures in this paper are available online at http://ieeexplore.ieee.org.

Digital Object Identifier 10.1109/TPEL.2016.2557964

commands based on the difference between the stator power and its reference signal. This has been addressed in several research works and known as DPC [12]–[16]. Similar to the DTC technique, the conventional DPC approach uses a predefined switching table to control the active and reactive power. An example of the implementation of this strategy was presented in [12] and revealed that the performance of such a method is mainly related to the stator flux position, which strongly depends on the stator resistance. The newly developed DPC approach avoids the use of switching tables and employs robust controllers to achieve better power quality with constant switching frequency. In [13], a nonlinear sliding mode control approach has been applied to calculate the required rotor voltage in the stator stationary frame. A simple PI controller with feedforward compensator is used in [14] to remove the steady-state error while, at the same time, a resonant controller is embedded in the loop to compensate for fifth and seventh current harmonics coming from the distortion of the grid voltage. The stability analysis of the entire closed-loop system is performed in [15] to come up with a simple PI controller without involving flux measurement and decoupling terms. Another variant of the DPC method is described in [16], where the required rotor voltage is calculated based on the estimated rotor flux. However, exact knowledge of the machine parameters is required to generate the reference of the rotor flux. Combined vector and DPC were presented in [17], and a complete overview about the control of DFIG can be found in [18]. In the majority of the aforementioned works, some challenges and improvements of DPC in controlling DFIG are demonstrated by simulation results, but, it is rarely that experimental tests have been conducted to demonstrate the feasibility of the proposed approaches, e.g., [12], [13], [15], and [17]–[22]. Recently, other controllers have been proposed to realize DPC, such as Backstepping control [23], where the performances of the controller are mainly based on the accuracy of the model parameters. Hence, zero steady-state error cannot be guaranteed under model uncertainties.

The model predictive control (MPC) is widely used for the DPC scheme, and it can provide a good overall performance. In MPC, the required rotor voltage is selected to optimize a cost function whose form depends on the performance specifications such as the minimization of the difference between the stator active and reactive powers, and their references [19]–[22], [24], [25]. An example of the MPC approach is to evaluate at each sampling time, the power error for all possible voltage vectors, and select the one which gives the lowest power error value over a predictive time [19]. For such a strategy, the predictive time is fixed to the sampling time, and the steady-state performance is enhanced by either using a small sampling time or/and arbitrarily adding an integral action, with a larger time constant, in the controller [5], [24], [25]. Such requirements raise concern about the design of these parameters. This issue is handled alternatively in this paper. To guarantee a fast transient response, while at the same time enhance the steady-state performance of DFIGs, this paper proposes a continuous-time model predictive DPC approach with a disturbance observer to compensate for the offset caused by model uncertainties and external disturbances [26]. The aim of this paper is to achieve

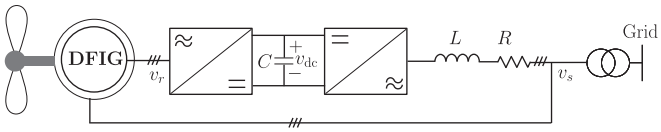

Fig. 1. DFIG-based WECS using back-to-back converters, with an L-type filter and a dc-link capacitor C.

independent stator active and reactive powers by means of stator current control. The idea behind the proposed strategy is to use Taylor series expansion to approximate a cost function minimizing the difference between the stator currents and their references. Such a methodology leads to a closed-form solution of the resulting optimization problem [27]. More specifically, it turns out that the resultant controller is almost equivalent to the existing MPC of DFIGs [5]; however, the prominent difference is in the predictive time being different from the sampling time. More interestingly, an integral controller arises naturally in the loop which is one of the salient features of this paper. A similar methodology is adopted in [28] to design an accurate control of a permanent magnet synchronous motor (PMSM), where a newly defined cost function is used to directly introduce an integral action in the controller. The main advantage of the proposed controller, in comparison to that developed for a PMSM, is that the disturbance rejection performance can be appropriately specified by an adequate design of a disturbance observer. Synchronous, supersynchronous, and subsynchronous operations of a 2-kW DFIG are experimentally examined under the proposed control scheme. Simulation results are also provided based on the parameters of a realistic WECS of 2-MW DFIG. It is worth to mention that the active/reactive power reference required to work at a specified operating point is mainly related to the dimensioning of the whole system including the converters.

II. System Description and DFIG Modeling

The DFIG-based WECS considered in this paper is depicted in Fig. 1. Assuming that the machine is balanced and using motor convention, the machine equations in the *dq* reference frame are given by [29]

$$\begin{cases} \dfrac{d\psi_{sdq}}{dt} = -R_s i_{sdq} - j\omega_s \psi_{sdq} + v_{sdq} \\ \dfrac{d\psi_{rdq}}{dt} = -R_r i_{rdq} - j\left(\omega_s - \omega_r\right)\psi_{rdq} + v_{rdq} \end{cases} \tag{1}$$

where ψ_{sdq}, i_{sdq}, and v_{sdq}, are given as follows:

$$\psi_{sdq} = \begin{bmatrix} \psi_{sd} \\ \psi_{sq} \end{bmatrix}, \quad i_{sdq} = \begin{bmatrix} i_{sd} \\ i_{sq} \end{bmatrix}, \quad v_{sdq} = \begin{bmatrix} v_{sd} \\ v_{sq} \end{bmatrix} \tag{2}$$

and ψ_{rdq}, i_{rdq}, and v_{rdq}, are expressed as follows:

$$\psi_{rdq} = \begin{bmatrix} \psi_{rd} \\ \psi_{rq} \end{bmatrix}, \quad i_{rdq} = \begin{bmatrix} i_{rd} \\ i_{rq} \end{bmatrix}, \quad v_{rdq} = \begin{bmatrix} v_{rd} \\ v_{rq} \end{bmatrix}. \tag{3}$$

Here, (ψ_{sd}, ψ_{sq}), (i_{sd}, i_{sq}), and (v_{sd}, v_{sq}) are the components of the stator flux ψ_s, current i_s, and voltage v_s, respectively,

in the *dq* reference frame, while (ψ_{rd}, ψ_{rq}), (i_{rd}, i_{rq}), and (v_{rd}, v_{rq}) represent the components of the rotor flux ψ_r, current i_r, and voltage v_r, respectively, in the *dq* reference frame. R_s, R_r, and ω_s, are, respectively, the stator and rotor resistance, and the synchronous angular frequency.

The rotor and stator fluxes are described in terms of rotor and stator currents as

$$\psi_{sdq} = L_s i_{sdq} + L_m i_{rdq}, \qquad \psi_{rdq} = L_r i_{rdq} + L_m i_{sdq}. \tag{4}$$

This leads to

$$i_{rdq} = \frac{\psi_{sdq} - L_s i_{sdq}}{L_m}, \qquad \psi_{rdq} = \frac{L_r}{L_m}\left(\psi_{sdq} - \sigma L_s i_{sdq}\right) \tag{5}$$

where $\sigma = 1 - \frac{L_m^2}{L_s L_r}$ represents the leakage factor. L_m, L_s, and L_r, represent the mutual inductance, the stator inductance, and the rotor inductance, respectively. From (1) to (5), it follows that

$$\begin{cases} \dfrac{di_{sd}}{dt} = -a i_{sd} + \omega_{sl} i_{sq} + b\psi_{sd} + c\omega_r \psi_{sq} + \dfrac{v_{sd}}{\sigma L_s} - \dfrac{L_m v_{rd}}{\sigma L_s L_r} \\ \dfrac{di_{sq}}{dt} = -a i_{sq} - \omega_{sl} i_{sd} + b\psi_{sq} - c\omega_r \psi_{sd} + \dfrac{v_{sq}}{\sigma L_s} - \dfrac{L_m v_{rq}}{\sigma L_s L_r} \end{cases} \tag{6}$$

where

$$\begin{aligned} a &= \frac{R_s L_r + L_s R_r}{\sigma L_s L_r}, \qquad b = \frac{R_r}{\sigma L_s L_r}, \qquad c = \frac{1}{\sigma L_s} \\ \omega_{sl} &= \omega_s - \omega_r. \end{aligned} \tag{7}$$

Here, ω_r and ω_{sl} represent the rotor and the slip angular frequency, respectively. The instantaneous active and reactive powers P_s and Q_s, generated at the stator side, can be written as a function of the stator voltages and currents as follows:

$$P_s = -\frac{3}{2}\left(v_{sd} i_{sd} + v_{sq} i_{sq}\right), \qquad Q_s = -\frac{3}{2}\left(v_{sq} i_{sd} - v_{sd} i_{sq}\right). \tag{8}$$

If the *q*-axis of the reference frame is aligned with the stator voltage, i.e., $v_{sq} = V_s$ and $v_{sd} = 0$, then, by neglecting the stator resistance, we obtain

$$\psi_s = \psi_{sd} \approx \frac{V_s}{\omega_s}, \qquad \psi_{sq} \approx 0. \tag{9}$$

Moreover, the expressions of P_s and Q_s in (8) can be simplified as follows:

$$P_s = -\frac{3}{2} V_s i_{sq}, \qquad Q_s = -\frac{3}{2} V_s i_{sd}. \tag{10}$$

Thus, knowing the magnitude V_s of the grid voltage, the stator active and reactive powers can be independently controlled by regulating the stator current components separately. Using (9), the equations describing these components become as

$$\begin{cases} \dfrac{di_{sd}}{dt} = -a i_{sd} + \omega_{sl} i_{sq} + b\dfrac{V_s}{\omega_s} - \dfrac{L_m}{\sigma L_s L_r}\left(v_{rd} - \delta_d\right) \\ \dfrac{di_{sq}}{dt} = -\omega_{sl} i_{sd} - a i_{sq} + c\dfrac{\omega_{sl} V_s}{\omega_s} - \dfrac{L_m}{\sigma L_s L_r}\left(v_{rq} - \delta_q\right) \end{cases} \tag{11}$$

where δ_d and δ_q are additive terms that represent model uncertainties and external disturbances. To simplify the controller design, it is assumed that

$$\lim_{t\to\infty} \dot{\delta}_d = 0, \qquad \lim_{t\to\infty} \dot{\delta}_q = 0. \tag{12}$$

III. Continuous-Time Model Predictive Control (CTMPC)

Although CTMPC has been successfully applied to electrical machines such as PMSMs [28], it has not been practically applied to DFIG. Recent advances in CTMPC have resulted in improving the steady-state performance [30], [31], and have made it to compete with other robust approaches. In CTMPC, the control objective is reduced to an optimization problem, where the performance requirement is formulated in terms of a cost function. For DFIG, the performance specifications can be achieved by the minimization of the following quadratic cost function

$$\Im = \int_0^{T_r} \left(e_d\left(t+\tau\right)\right)^2 d\tau + \int_0^{T_r} \left(e_q\left(t+\tau\right)\right)^2 d\tau \tag{13}$$

where T_r is the predictive time. The tracking errors e_d and e_q are described in terms of the stator currents components and their references $i_{sd\text{ref}}$ and $i_{sq\text{ref}}$ as follows:

$$\begin{cases} e_d\left(t+\tau\right) = i_{sd\text{ref}}\left(t+\tau\right) - i_{sd}\left(t+\tau\right) \\ e_q\left(t+\tau\right) = i_{sq\text{ref}}\left(t+\tau\right) - i_{sq}\left(t+\tau\right). \end{cases} \tag{14}$$

In CTMPC, the future behavior of each of the tracking errors is predicted using Taylor series expansion up to the relative degree with respect to the input. Here, the inputs are the rotor voltage components. From (11), it is clear that the relative degree corresponding to each output is equal to unity. By considering Taylor series expansion up to 1, we obtain

$$\begin{cases} e_d\left(t+\tau\right) = e_d\left(t\right) + \tau\left(\dfrac{di_{sd\text{ref}}}{dt} - \dfrac{di_{sd}}{dt}\right) \\ e_q\left(t+\tau\right) = e_q\left(t\right) + \tau\left(\dfrac{di_{sq\text{ref}}}{dt} - \dfrac{di_{sq}}{dt}\right). \end{cases} \tag{15}$$

Following Yang *et al.* [31], substituting (15) into (13), together with (11), results in a quadratic cost function, dependent on the inputs v_{dr} and v_{qr}, which gives the optimal closed-form solution as follows:

$$\begin{cases} v_{rd}^* = -\dfrac{\sigma L_s L_r}{L_m}\left(\dfrac{3}{2T_r} e_d + \dfrac{di_{sd\text{ref}}}{dt} + A_d\right) + \delta_d \\ v_{rq}^* = -\frac{\sigma L_s L_r}{L_m}\left(\dfrac{3}{2T_r} e_q + \dfrac{di_{sq\text{ref}}}{dt} + A_q\right) + \delta_q \end{cases} \tag{16}$$

where

$$\begin{cases} A_d = a i_{sd} - \omega_{sl} i_{sq} - b\dfrac{V_s}{\omega_s} \\ A_q = \omega_{sl} i_{sd} + a i_{sq} - c\dfrac{\omega_{sl} V_s}{\omega_s}. \end{cases} \tag{17}$$

Now, substituting the control law (16), (17) into (11), gives the closed-loop system error equations as follows:

$$\dot{e}_d = -\frac{3}{2T_r} e_d, \qquad \dot{e}_q = -\frac{3}{2T_r} e_q. \tag{18}$$

Therefore, the predictive time T_r can be selected based on the desired rise time. As the information about the disturbances is

not available for direct measurement, the lumped disturbance $\delta_{d,q}$ is replaced by its estimate $\hat{\delta}_{d,q}$ in the control law. Such a requirement reveals the need for a disturbance observer.

IV. Disturbance Observer

A disturbance observer proposed in [26] can be considered as an adequate candidate for estimating unmeasurable disturbances. For the DFIG, the disturbance observer is given by

$$\begin{cases} \dot{\hat{\delta}}_d = -\dfrac{L_m l_d}{\sigma L_s L_r}\hat{\delta}_d + l_d\left(\dfrac{di_{sd}}{dt} + A_d + \dfrac{L_m v_{rd}}{\sigma L_s L_r}\right) \\ \dot{\hat{\delta}}_q = -\dfrac{L_m l_q}{\sigma L_s L_r}\hat{\delta}_q + l_q\left(\dfrac{di_{sq}}{dt} + A_q + \dfrac{L_m v_{rq}}{\sigma L_s L_r}\right) \end{cases} \tag{19}$$

where l_d and l_q are the observer gains. By considering (11) and (19), the dynamics of the estimation errors $e_{\delta_d} = \hat{\delta}_d - \delta_d$ and $e_{\delta_q} = \hat{\delta}_q - \delta_q$ are governed by

$$\dot{e}_{\delta d} = -\frac{L_m l_d}{\sigma L_s L_r}e_{\delta d} + \dot{\delta}_d, \qquad \dot{e}_{\delta q} = -\frac{L_m l_q}{\sigma L_s L_r}e_{\delta q} + \dot{\delta}_q. \tag{20}$$

With the assumption (12), one can conclude that the disturbance estimation error system can be made asymptotically stable by choosing the observer gains such that $l_d > 0$ and $l_q > 0$. More specifically, under a step disturbance, the estimate tracks the actual disturbance within a time constant of $\frac{\sigma L_s L_r}{l_{d,q} L_m}$. Furthermore, with a view to avoid practical problems that may arise because of the time derivative of the stator current components, one can further simplify the proposed disturbance observer. Indeed, assuming that $\delta_{d,q}(0) = 0$, and substituting the control law (16), (17) into the disturbance observer (19) yields

$$\begin{cases} \hat{\delta}_d = -\dfrac{3l_d}{2T_r}\displaystyle\int_0^t e_d(\tau)\,d\tau - l_d e_d(t) + l_d e_d(0) \\ \hat{\delta}_q = -\dfrac{3l_q}{2T_r}\displaystyle\int_0^t e_q(\tau)\,d\tau - l_q e_q(t) + l_q e_q(0). \end{cases} \tag{21}$$

Hence, an integral action is naturally introduced in the controller, rather than arbitrarily adding an integral term to the rotor voltage command. Such a modification guarantees zero steady-state error despite parameter variations and unknown disturbances. The majority of the existing disturbance observers requires the integration of the system model to estimate an external disturbance. In other words, the integration of the error between the actual and the estimated measurement is usually used to generate the disturbance estimation. In our case, the estimate is driven by the tracking error $e_{d,q}$, i.e., the error between the stator current components and their references, which makes the composite controller more convenient for a practical implementation.

V. Stability of the Overall Closed-Loop System

Neglecting the initial tracking error $e_{d,q}(0)$, the composite controller consisting of the CTMPC (16), (17) and the disturbance observer (21) is given by

$$\begin{cases} v_{rd}^* = -\dfrac{\sigma L_s L_r}{L_m}\left(K_{pd}e_d(t) + K_{id}\displaystyle\int_0^t e_d(\tau)\,d\tau + N_d\right) \\ v_{rq}^* = -\dfrac{\sigma L_s L_r}{L_m}\left(K_{pq}e_q(t) + K_{iq}\displaystyle\int_0^t e_q(\tau)\,d\tau + N_q\right) \end{cases} \tag{22}$$

where

$$K_{pd} = \frac{3}{2T_r} + \frac{L_m l_d}{\sigma L_s L_r}, \qquad K_{pq} = \frac{3}{2T_r} + \frac{L_m l_q}{\sigma L_s L_r} \tag{23}$$

and

$$K_{id} = \frac{3L_m l_d}{2T_r \sigma L_s L_r}, \qquad K_{iq} = \frac{3L_m l_q}{2T_r \sigma L_s L_r}. \tag{24}$$

The predictive terms N_d and N_q are given by

$$\begin{cases} N_d = \dfrac{di_{sd\text{ref}}}{dt} + a i_{sd} - \omega_{sl} i_{sq} - b\dfrac{V_s}{\omega_s} \\ N_q = \dfrac{di_{sq\text{ref}}}{dt} + \omega_{sl} i_{sd} + a i_{sq} - c\dfrac{\omega_{sl} V_s}{\omega_s}. \end{cases} \tag{25}$$

For the closed-loop system analysis, substituting (22) into the system dynamics (11) gives

$$\begin{cases} K_{id}\int_0^t e_d(\tau)\,d\tau + K_{pd}e_d(t) + \dot{e}_d(t) = -\dfrac{\sigma L_s L_r}{L_m}\delta_d \\ K_{iq}\int_0^t e_q(\tau)\,d\tau + K_{pq}e_q(t) + \dot{e}_q(t) = -\dfrac{\sigma L_s L_r}{L_m}\delta_q. \end{cases} \tag{26}$$

The poles associated with the above closed-loop error equations are given by

$$s_{1(d,q)} = -\frac{3}{2T_r}, \qquad s_{2d} = -\frac{L_m l_d}{\sigma L_s L_r}, \qquad s_{2q} = -\frac{L_m l_q}{\sigma L_s L_r}. \tag{27}$$

Since the predictive time and the observer gains are positives, the closed-loop system is stable, indicating that the tracking errors are bounded. Additionally, the assumption in (12) guarantees that the system output tracks its reference with an error, which eventually converges to zero as time tends to infinity. More specifically, the reference-to-output transfer function $H(s)$, for a constant set-point, can be expressed by

$$H(s) = \frac{\left(\frac{3}{2T_r} + \frac{L_m l_{d,q}}{\sigma L_s L_r}\right)s + \frac{3L_m l_{d,q}}{2\sigma T_r L_s L_r}}{s^2 + \left(\frac{3}{2T_r} + \frac{L_m l_{d,q}}{\sigma L_s L_r}\right)s + \frac{3L_m l_{d,q}}{2\sigma T_r L_s L_r}}. \tag{28}$$

Remark 1: The parameters of the composite controller can be chosen according to the desired pole locations (27). In fact, in order to have a fast transient response, the predictive time T_r should be chosen as small as possible to ensure a good tracking performance, while the observer gain $l_{d,q}$ should be chosen large enough to guarantee a fast disturbance rejection. From a practical standpoint, either decreasing T_r and/or increasing $l_{d,q}$ will eventually correspond to an amplification of the measurement noise. Therefore, a tradeoff should be made when designing the parameters of the composite controller to prevent large magnification of the measurement noise.

Remark 2: The required rotor voltage is calculated based on the predictive current model over the specified predictive time.

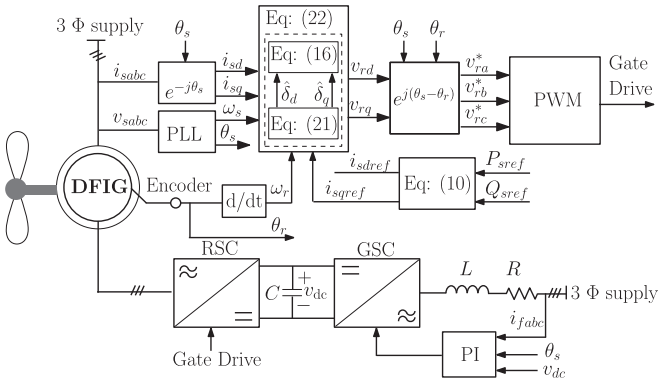

Fig. 2. Block diagram of the proposed controller for a DFIG-based WECS.

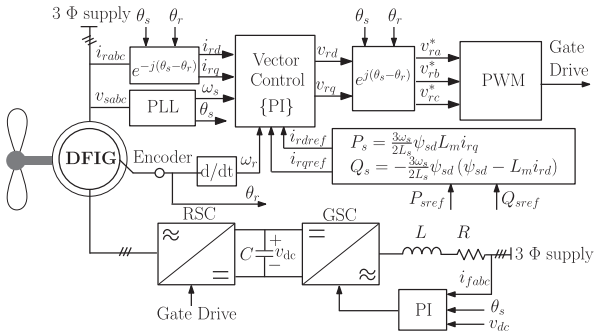

Fig. 3. Block diagram of the VC scheme for a DFIG-based WECS.

Unlike the conventional MPC of DFIG [5], [24], the predictive time is not fixed to the sampling time, and it can be chosen based on the desired settling time. Moreover, the integral controller can be specified by setting the observer gains to correspond to the desired disturbance rejection performance, which is different from the existing MPC for DFIG, where a relatively large time constant is usually selected for the integral action.

Remark 3: As the initial tracking error $e_{d,q}(0)$ is not considered in the composite controller (22), the nominal transient performance, defined by (18), may not be preserved when dealing with a step input because of the introduction of the integral action. More specifically, the transient performance, in response to a step input, will be governed by the transfer function given by (28). To guarantee a good dynamic response, the power reference can be realized using a first-order low-pass filter to have zero initial tracking error, i.e., $e_{d,q}(0) = 0$. Such a strategy allows exploring the capability of the controller to achieve a good tracking performance, while at the same time, to reduce the magnitude of the rotor voltage during transients.

VI. Computer Simulations

A. Control Loop Diagram

Simulation studies have been carried out using MATLAB/Simulink software package to verify the performance of the proposed controller compared to the conventional VC scheme. A block diagram for the implementation of the proposed CTMPC-based DPC is depicted in Fig. 2. In this configuration, a phase-locked loop (PLL), as described in [32], is used to compute the reference angle θ_s for the synchronous reference frame. The stator currents are measured and transformed to *dq* frame in which the controller is designed. The stator current references are computed directly from the desired active and reactive powers, and the magnitude V_s of the grid voltage, without involving the machine parameters or the rotor currents. The required rotor voltage is calculated based on the stator current error and, then, transformed into the rotor reference frame. Finally, a PWM technique is used to control the semiconductor switches of the RSC based on the rotor voltage commands.

By controlling the current flowing through the line filter, the dc-link voltage is maintained constant and is regulated at a desired voltage reference. The controller of the GSC consists of a conventional cascaded scheme using two PI controllers [7]. Such a control scheme is not described here, as the main focus is given on the control of RSC of DFIG. It is noticed that all simulation tests, given in this section, were performed using 2-MW DFIG with the rotor speed $\Omega_r = 1200$ r/min. In addition, sinusoidal PWM technique is adopted to realize the rotor voltage commands. The system parameters of 2-MW DFIG are listed in Table I in the Appendix.

The sampling frequency is set to be equal to 6.25 kHz, while the switching frequency is chosen equal to 3.125 kHz. A time step of 5 μs was used to discretize the DFIG model. The predictive time can be selected based on the performance specifications. Following the above remarks, the predictive time T_r is set equal to 5 ms. The observer gains l_d and l_q are both set to be 0.005 so that the time constant of the disturbance observer is equal to $\tau_o = \frac{\sigma L_s L_r}{l_{d,q} L_m} = 28$ ms.

B. Dynamic Performance Under Nominal Parameters

First test was performed to compare the proposed controller CTMPC with the conventional VC scheme, which is given in Fig. 3, under nominal parameters. The VC scheme uses a PI controller to regulate the stator active and reactive powers through the control of the rotor current components. To have a fair comparison, the parameters of the PI controller are tuned using internal model control [33] so that both controllers provide similar current closed-loop bandwidth under nominal parameters.

Figs. 4 and 5 compare the dynamic performance of both controllers using the nominal parameters. In Fig. 4, the active power was suddenly stepped up from zero to 0.75 per unit (p.u.), while the reference of the reactive power was kept equal to zero. In Fig. 5, the active power was maintained equal to zero, with the reactive power stepped up from zero to 0.75 p.u. From the results, it can be concluded that both controllers are capable of producing a fast dynamic response, within the specified settling time. However, it is clear that the use of a filtered reference allows achieving a good dynamic performance under the proposed controller, as mentioned in Remark 3.

C. Steady-State Performance Under Model Uncertainty

This test was performed to compare the steady-state performance of the proposed controller with that of the VC scheme

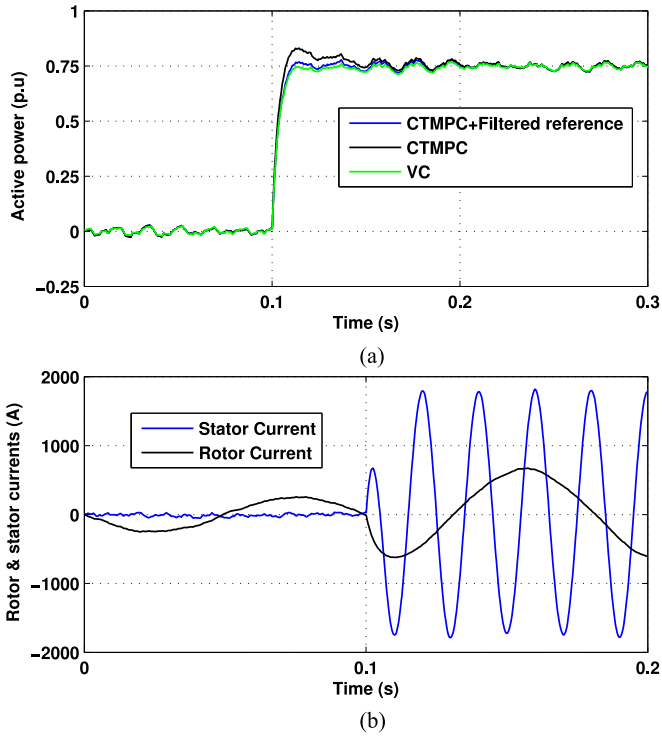

Fig. 4. Response to a step change in active power under nominal model, and with $\Omega_r = 1200$ r/min using 2-MW DFIG, where VC and CTMPC denote VC and CTMPC, respectively. (a) Active power. (b) Current response under CTMPC.

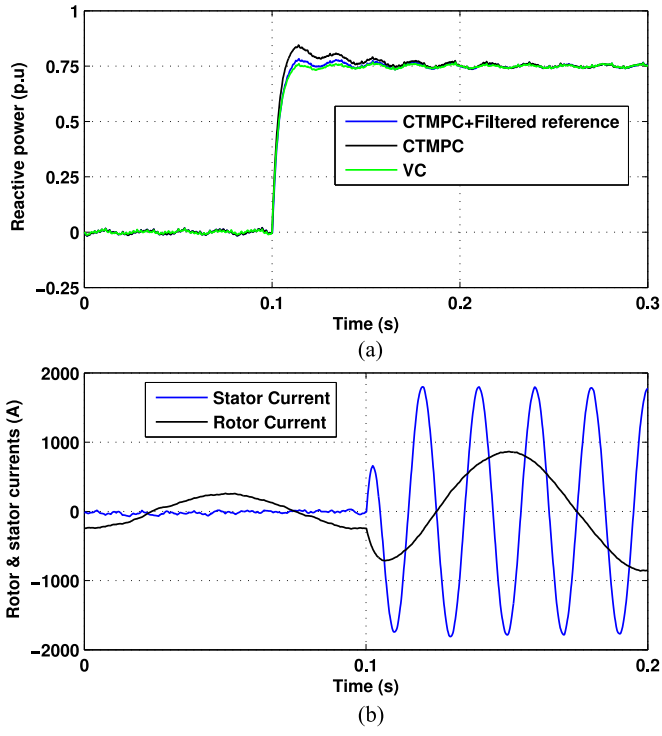

Fig. 5. Response to a step change in reactive power under nominal model, and with $\Omega_r = 1200$ r/min using 2-MW DFIG, where VC and CTMPC denote VC and CTMPC, respectively. (a) Reactive power. (b) Current response under CTMPC.

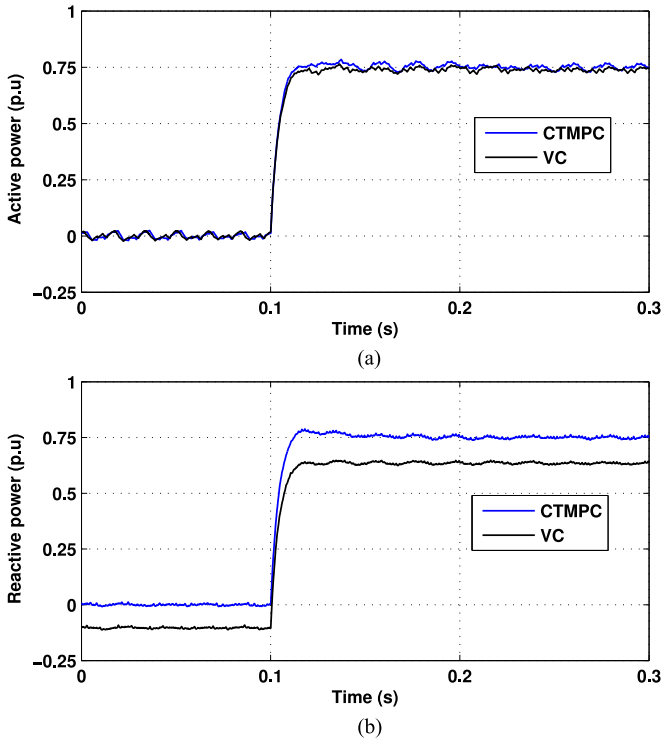

Fig. 6. Response to a step change ($0 \rightarrow 0.75$ p.u.) in active and reactive powers under model uncertainty, and with $\Omega_r = 1200$ r/min using 2-MW DFIG, where VC and CTMPC denote VC and CTMPC, respectively. (a) Active power. (b) Reactive power.

under model uncertainty. To this end, the mutual inductance L_m and the stator self-inductance l_s were incorrectly set in both controllers, and their values were set to be equal to 150% and 50% of their nominal values, respectively.

Moreover, two simulation tests were performed to compare the performances of both controllers. First, the active power was stepped up from zero to 0.75 p.u. at $t = 0.1$ s, while the reactive power was kept null, and the corresponding results are given in Fig. 6(a). The second test consists of stepping up the reactive power, while maintaining the active power equal to zero as shown in Fig. 6(b). Fig. 7 represents the power tracking error for both controllers. As seen, a larger steady-state error is observed with the VC scheme, especially, for the reactive power control. This is because the VC scheme cannot guarantee the zero steady-state error under parameter variations. As shown in Fig. 3, the steady-state performance of the VC scheme can be improved by adding an external loop to generate the rotor current components based on the power error. However, such a modification may impact the closed-loop bandwidth, and may complicate the design process.

VII. Experimental Results

Fig. 8 shows the test bed setup used to experimentally verify the effectiveness of the proposed approach. The system comprises a 2-kW DFIG coupled to a controlled induction motor that plays the role of a wind turbine emulator. The system parameters of 2-kW DFIG are listed in Table II in the Appendix. An

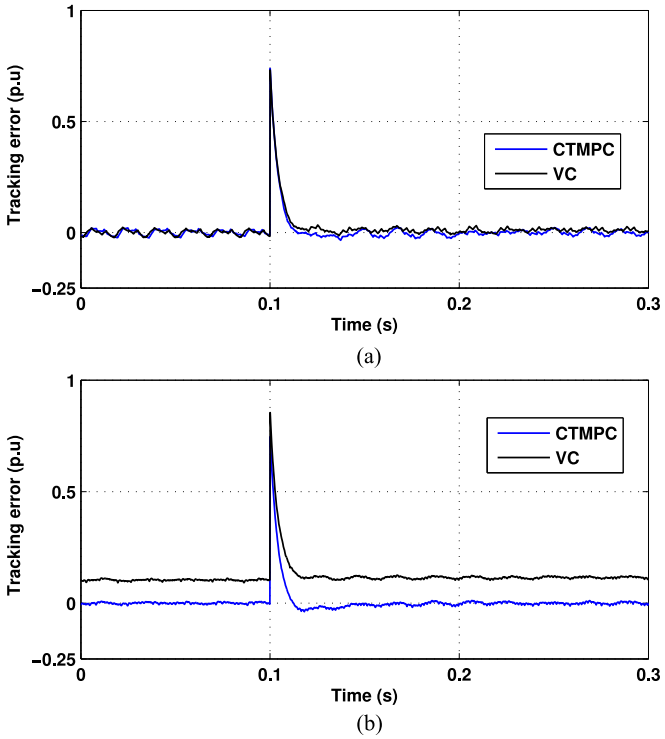

Fig. 7. Tracking errors following a step change in active and reactive powers under model uncertainty, and with $\Omega_r = 1200$ r/min using 2-MW DFIG, where VC and CTMPC denote VC and CTMPC, respectively. (a) Active power error. (b) Reactive power error.

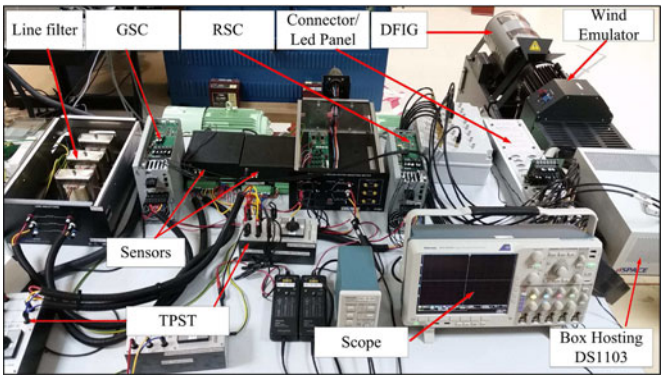

Fig. 8. Experimental setup for testing the 2-kW DFIG system.

incremental encoder is employed to measure the rotor position/speed. The stator windings are directly connected to the grid, whereas the GSC is supplied through a line filter from the grid. Both RSC and GSC are controlled by a dSPACE DS1103 DSP board, which is equipped with Power PC 750GX (Master processor) running at 1 GHz, and a Texas Instruments TMS320F240 DSP (slave processor) running at 20 MHz.

The sampling and the switching frequencies are chosen similar to that used for the simulation of a 2-MW DFIG. The observer gains l_d and l_q are chosen so that the time constant of the observer gain is about 41 ms, while the predictive time is set to be equal to 1 ms. Hence, following (28), the active/reactive

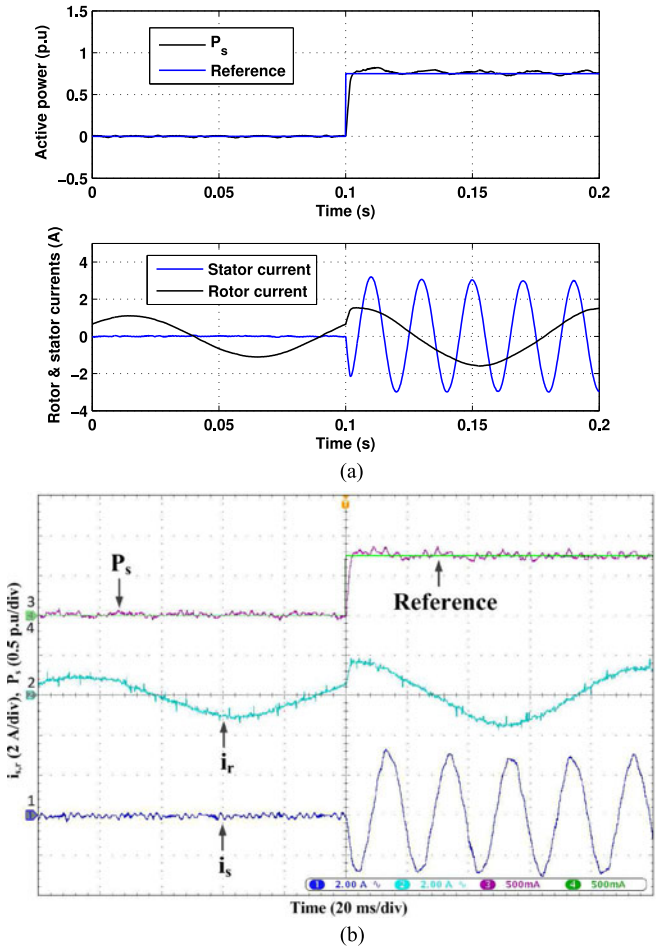

Fig. 9. Response to a step change in active power under nominal model, and with $\Omega_r = 1200$ r/min, i_s (2 A/div), i_r (2 A/div), and P_s (0.5 p.u./div). (a) Simulation results. (b) Experimental results.

power will need about 2.3 ms to reach its reference. The switching actions for both RSC and GSC are generated using the third harmonic injection PWM technique [34]. Several tests were conducted to experimentally verify the performance of the proposed controller. However, only some simulation results with 2-kW DFIG are provided to be compared with the experimental results, using the same scaling, in order to show the consistency between the simulation and the experimental results. Moreover, it is noticed that only the CTMPC is tested experimentally, as it is clear that the VC scheme given in Fig. 3 suffers from a lack of robustness to parameter variation, although it can offer a good dynamic performance.

A. Dynamic Performance Under Nominal Model and Change in Active and Reactive Powers

This experiment was performed to verify the dynamic performance of the closed-loop system under the proposed controller. Two experimental tests were conducted, separately, with a step change in active and reactive powers. In the first test, a step change in the active power was applied as $P_s = 0 \rightarrow 0.75$ p.u., while the reactive power remained null, and the corresponding

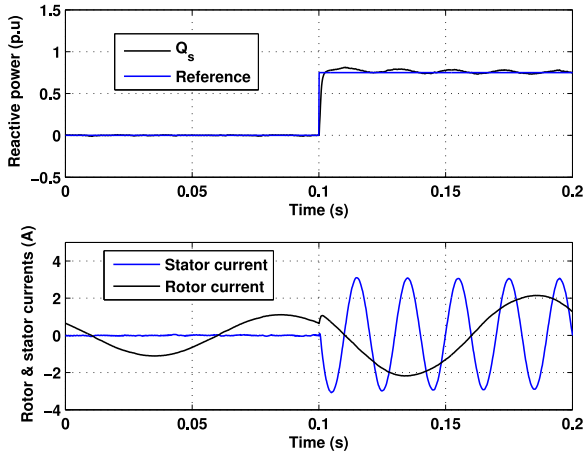

(a)

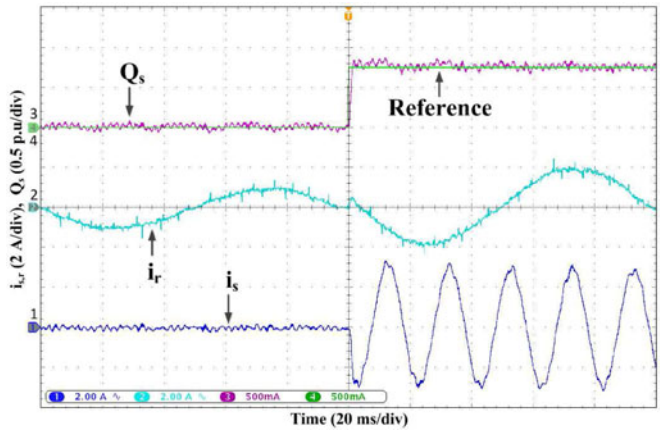

(b)

Fig. 10. Response to a step change in reactive power under nominal model, and with $\Omega_r = 1200$ r/min, i_s (2 A/div), i_r (2 A/div), and Q_s (0.5 p.u./div). (a) Simulation results. (b) Experimental results.

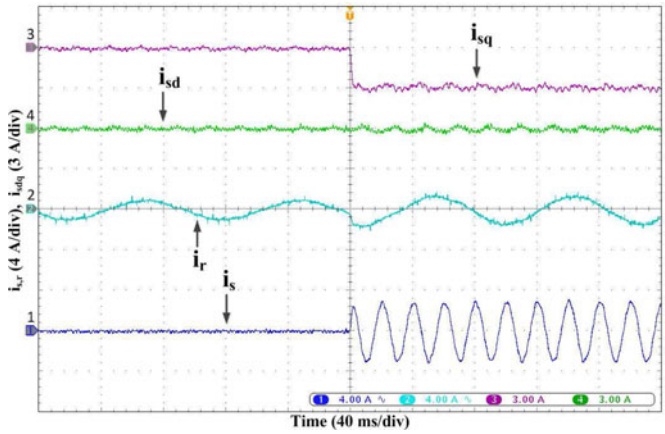

Fig. 11. Response to a step change in active power under model uncertainty, and with $\Omega_r = 1200$ r/min, i_s (4 A/div), i_r (4 A/div), i_{sq} (3 A/div), and i_{sd} (3 A/div).

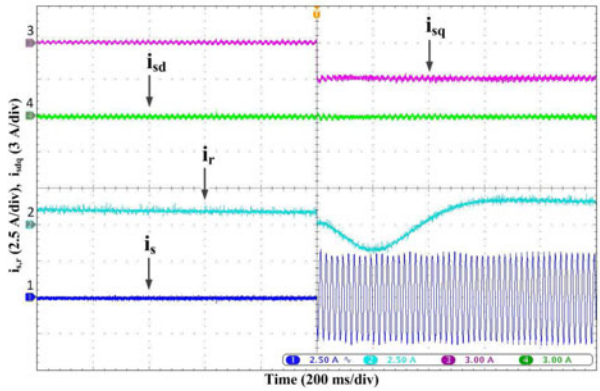

Fig. 12. Response to a step change in active power under model uncertainty, and with $\Omega_r = 1500$ r/min, i_s (4 A/div), i_r (4 A/div), i_{sq} (3 A/div), and i_{sd} (3 A/div).

results are given in Fig. 9. In the second test, the active power was kept equal to zero, while the reactive power Q_s was stepped up from zero to 0.75 p.u., as shown in Fig. 10. It can be observed from the experimental results that the active and reactive powers took about 3 ms to reach their references with zero steady-state error, which is consistent with the theoretical analysis. Moreover, the current waveforms confirmed the simulation results shown in Figs. 9(a) and 10(a).

B. Dynamic and Steady-State Performances Under Model Uncertainty and Change in Active Power

Here, the dynamic performance of the system using the proposed controller was tested in response to a step change in active power at different DFIG operating speeds including the synchronous speed. In this case, the *d*-axis stator current reference was kept null, while the *q*-axis stator current reference was suddenly stepped down from zero to -3 A, i.e., $Ps = 1.5$ kW $= 0.75$ p.u. In addition, to test the robustness of the closed-loop system, the resistances and the inductances of the DFIG model used in the controller are set to be 75% and 50% of their actual values, respectively.

As seen from Figs. 11–13, the *q*-axis stator current rapidly reaches its new steady-state value in response to a step change. The stator current components are with neither steady-state error nor overshoot. The settling time is within a few milliseconds, which is consistent with the theoretical analysis. Also, the results show that the *d*-axis stator current is maintained equal to zero, meaning that the stator reactive power is well controlled. More interestingly, it can be observed from these plots that a decoupled control of active and reactive power is outstandingly achieved. It is worth noting that, under synchronous speed, the rotor current is constant, as the slip frequency is null. However, a significant reduction in the rotor current observed in Fig. 12, after applying a step change in active power, is caused by an abrupt drop in rotor speed. Such a transient behavior indicates that the active power is viewed as a load torque that is suddenly applied on the wind emulator. As a result, the speed of the wind turbine emulator decreases and returns back to its steady-state condition. Furthermore, Fig. 13 shows that the experimental results are almost similar to that obtained with the simulation. It is noticed that the fluctuation observed with the experimental results are due to the measurement noise.

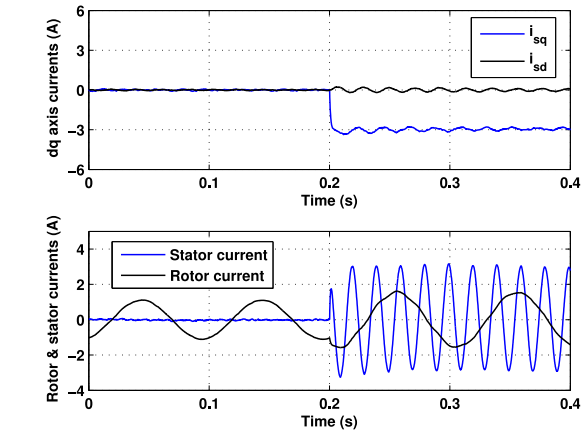

(a)

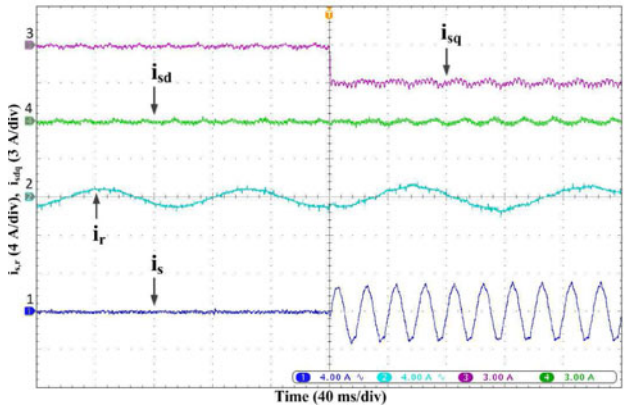

(b)

Fig. 13. Response to a step change in active power under model uncertainty, and with $\Omega_r = 1800$ r/min, i_s (4 A/div), i_r (4 A/div), i_{sq} (3 A/div), and i_{sd} (3 A/div). (a) Simulation results. (b) Experimental results.

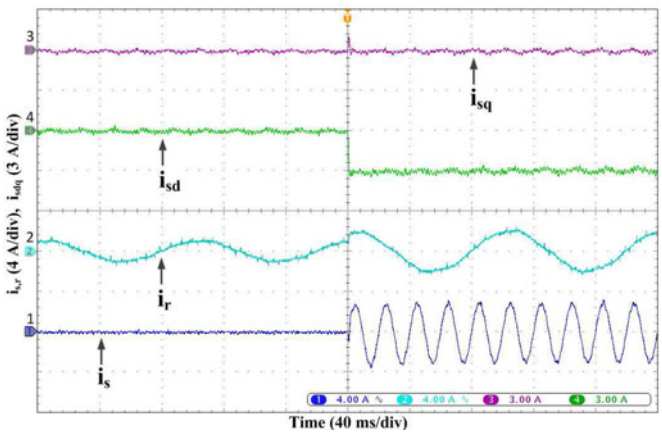

Fig. 14. Response to a step change in reactive power under model uncertainty, and with $\Omega_r = 1200$ r/min, i_s (4 A/div), i_r (4 A/div), i_{sq} (3 A/div), and i_{sd} (3 A/div).

C. Dynamic and Steady-State Performances Under Model Uncertainty and Change in Reactive Power

Tests under changes in reactive power have also been conducted with the active power maintained equal to zero, and Figs. 14–16 show the corresponding results for supersynchronous, subsynchronous, and synchronous speed, respec-

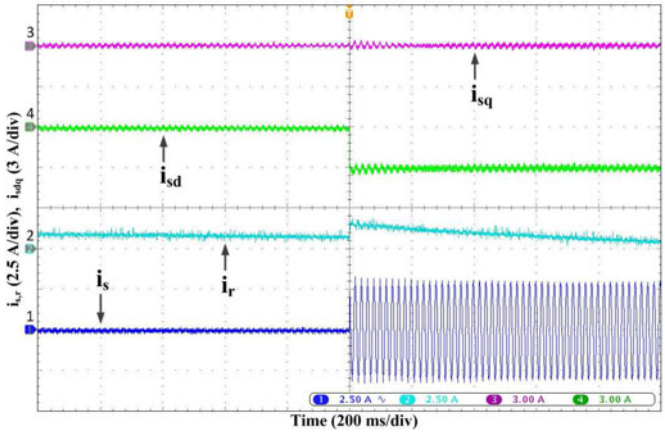

Fig. 15. Response to a step change in reactive power under model uncertainty, and with $\Omega_r = 1500$ r/min, i_s (4 A/div), i_r (4 A/div), i_{sq} (3 A/div), and i_{sd} (3 A/div).

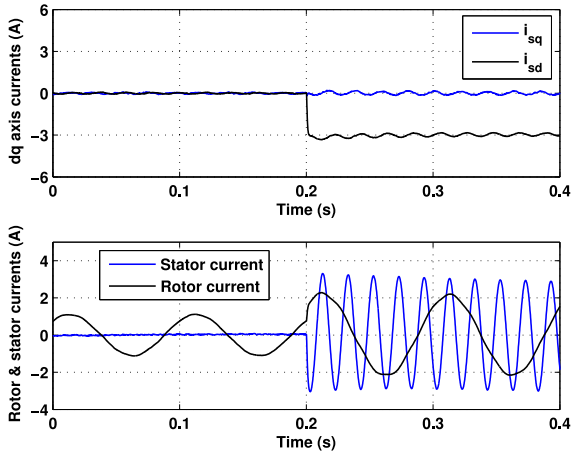

(a)

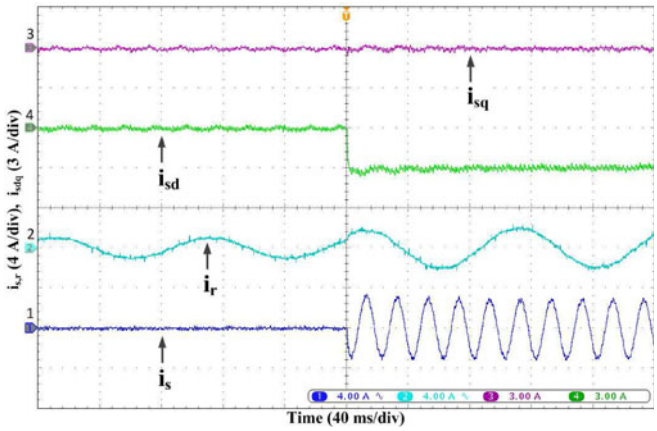

(b)

Fig. 16. Response to a step change in reactive power under model uncertainty, and with $\Omega_r = 1800$ r/min, i_s (4 A/div), i_r (4 A/div), i_{sq} (3 A/div), and i_{sd} (3 A/div). (a) Simulation results. (b) Experimental results.

tively. In this experiment, the resistances and the inductance are set to be equal to 150% of their actual values. As seen, the d-axis stator current reference was stepped from zero to -3 A to regulate the stator reactive power at $Q_s = 1.5$ kVar. Obviously, the q-axis stator current is regulated to zero.

From the results, it can be seen that the active power is robust to changes in reactive power, and clearly, the d-axis current jumps suddenly from zero to the desired steady-state value, meaning that the change in reactive power can be realized almost instantaneously, which can be treated as an ancillary service for a wind turbine. Similar to the previous test, it is clear that the proposed approach results in a decoupled active and reactive power. Also, Fig. 16 illustrates the consistency between the real-time implementation and the numerical simulation.

D. Performance Evaluation Under Rotor Speed Variation

In this test, a step change in reactive power is examined with a rotor speed variation, while at the same time, the DFIG keeps supplying the grid with a constant active power of 1.5 kW. A step change in reactive power was done at the instant when the speed crosses the synchronous one. In fact, the d-axis stator current is suddenly changed from 3 to -2 A. This allows testing the proposed approach for both inductive and capacitive reactive power exchange with the grid, depending on whether the DFIG operates at subsynchronous or supersynchronous speed. The rotor speed change takes place at $t = 0.4$ s, and it reaches its new steady-state value at $t = 1.6$ s. Here, the observer gain is taken equal to 0.05. From Fig. 17, it is clear that both steady state and the transient performances are satisfactory. The current behavior produced with the numerical simulation is also closely matched with experimental results.

E. Disturbance Rejection Under Sudden Change in Rotor Speed

This test was performed to investigate the influence of the disturbance observer of the composite controller and its behavior in response to an abrupt uncertainty in the speed measurement. In other words, the speed measurement was suddenly and incorrectly set in the controller to mimic an abrupt disturbance, which allows evaluating the disturbance rejection capability of the composite controller. This is because it is not possible to realize practically a sudden change in the rotor speed. In such a situation, the steady-state values of the rotor voltage components, provided by the composite controller, should be kept constant under speed measurement error to guarantee accurate control of the active/reactive power. This test permits also to investigate the transient response of the disturbance observer and how it adapts to improve the steady-state performance. Moreover, two values of $l_{d,q}$ are used to illustrate the consistency between the experimental results and the theoretical analysis. The experiment was performed under a constant active power of 1.5 kW, i.e., $i_{sq} = -3$ A, with $\Omega_r = 1200$ r/min. The rotor speed value is suddenly increased in the controller from $1200 \rightarrow 1300$ r/min.

As shown in Fig. 18, a large steady-state error is observed in the q-axis current response just after introducing an uncertainty

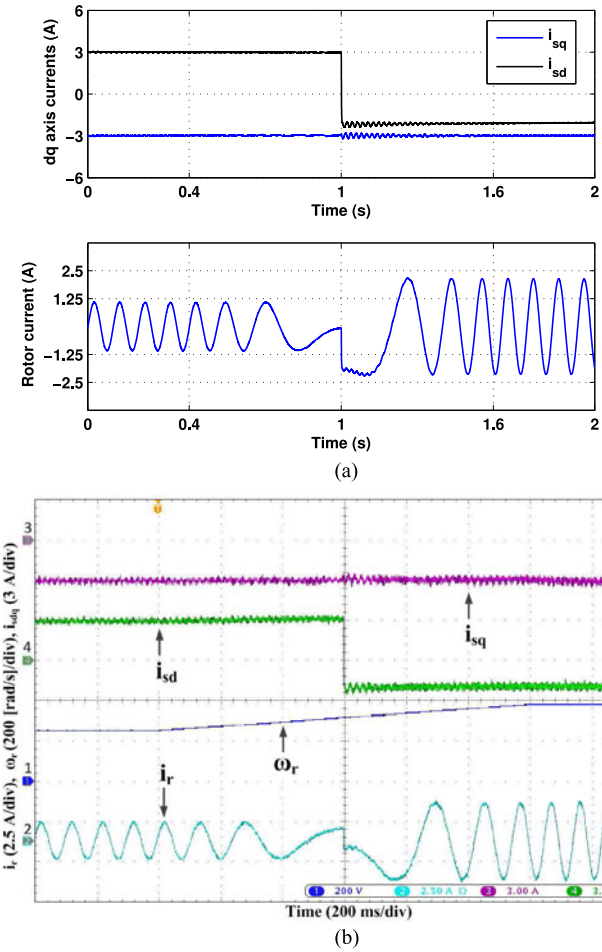

Fig. 17. Response to a step change in reactive power at synchronous speed during rotor speed variation (from 1200 to 1800 r/min), ω_r (200 [rad/s]/div), i_r (2.5 A/div), i_{sq} (3 A/div), and i_{sd} (3 A/div). (a) Simulation results. (b) Experimental results.

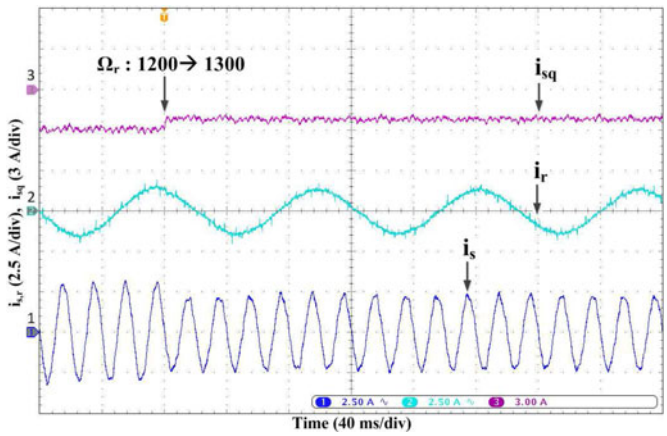

Fig. 18. Response to a sudden change in the rotor speed in the controller without the use of a disturbance observer, with $\Omega_r = 1200$ r/min, i_s (2.5 A/div), i_r (2.5 A/div), and i_{sq} (3 A/div).

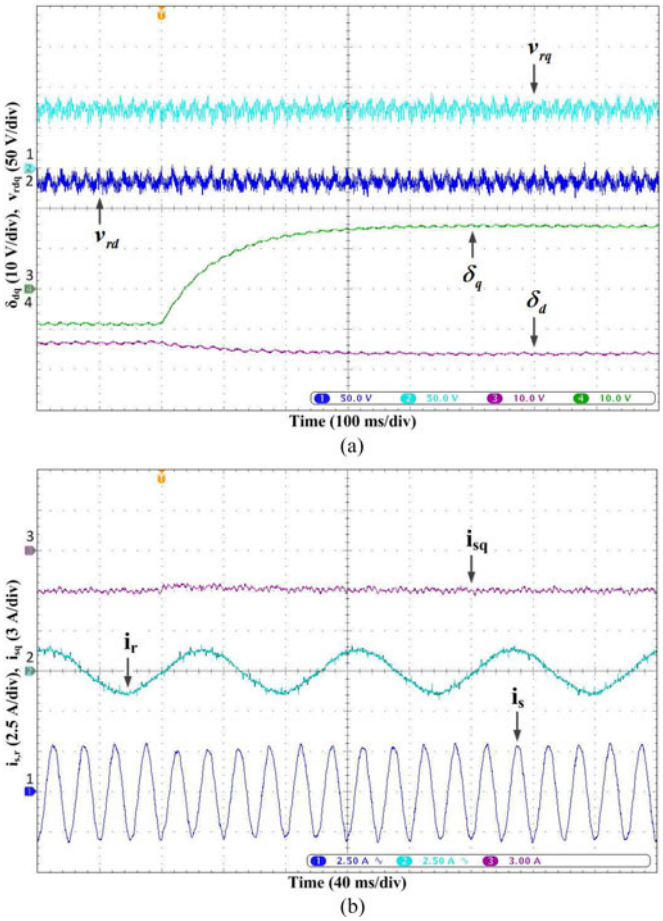

Fig. 19. Response to a sudden change in the rotor speed in the controller, with $\Omega_r = 1200$ r/min, and $l_{d,q} = 0.5$. (a) *dq* rotor voltage and disturbance estimation, v_{rd} (50 V/div), v_{rq} (50 V/div), δ_d (10 V/div), and δ_q (10 V/div). (b) current behavior, i_s (2.5 A/div), i_r (2.5 A/div), and i_{sq} (3 A/div).

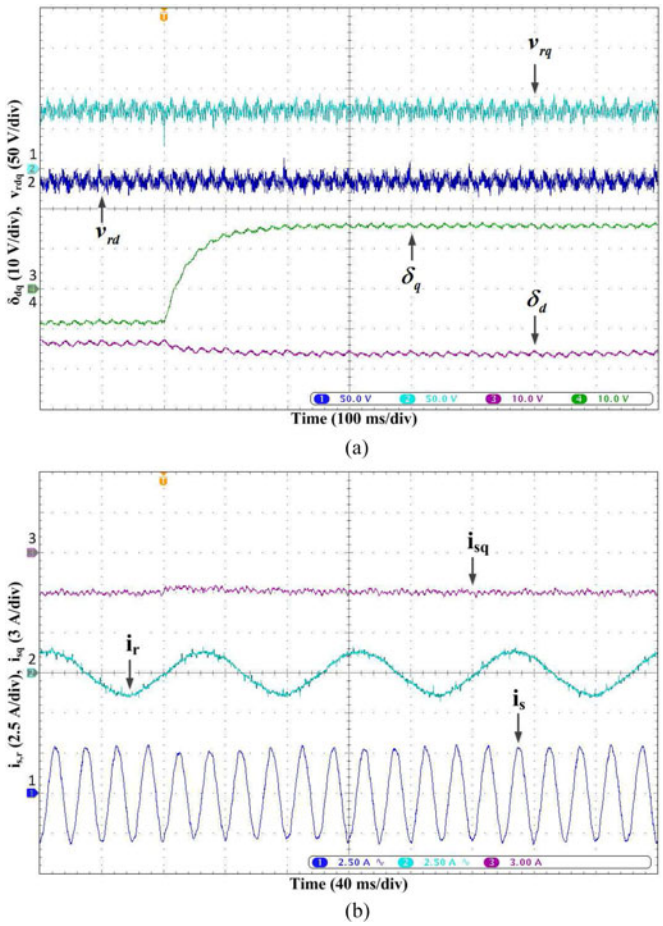

Fig. 20. Response to a sudden change in the rotor speed in the controller, with $\Omega_r = 1200$ r/min, and $l_{d,q} = 1$. (a) *dq* rotor voltage and disturbance estimation, v_{rd} (50 V/div), v_{rq} (50 V/div), δ_d (10 V/div), and δ_q (10 V/div). (b) current behavior, i_s (2.5 A/div), i_r (2.5 A/div), and i_{sq} (3 A/div).

on the speed measurement due to the absence of a disturbance observer. However, it can be seen from Figs. 19 and 20 that the steady-state error is quickly eliminated. This is because the estimated $\delta_{d,q}$ converges to a stable steady-state condition that keeps the rotor voltage components constant by compensating the effect of the speed measurement uncertainty.

More interestingly, by considering the limited accuracy of the model parameters, it can be observed that the estimate reaches its new steady-state status within a time constant that is approximately equal to $\frac{\sigma L_s L_r}{l_{d,q} L_m}$, which is consistent with the design process of the disturbance observer.

VIII. Conclusion

A robust continuous-time model predictive control (RCTMPC) for DFIG has been presented. The proposed approach directly calculates the rotor voltage commands based on the predictive stator current in the synchronous reference frame. The base line controller is derived based on the minimization of a quadratic cost function consisting of the error between the stator current components and their references. The RCTMPC has been combined with a disturbance observer to enhance the steady-state performance in the presence of model uncertainty and external perturbations.

The performance of the closed-loop system under the proposed controller is experimentally validated using a grid-connected DFIG. The proposed controller offers excellent behavior under synchronous, subsynchronous, and supersynchronous modes and also works very well under model uncertainties. Unlike the existing MPC for DFIG, the predictive time is not fixed to the sampling time, and it depends on the desired dynamic performance. Moreover, an integral action arises naturally in the composite controller, rather than directly introducing it into the control loop. Under suitable design parameters, good transient and steady-state performances can be obtained without having additional current control loop as for the VC scheme.

Appendix

The parameters values of the tested DFIGs are given in the following table.

TABLE I
PARAMETERS VALUES OF THE 2 MW DFIG

Rated power	2 MW
Stator voltage	690 V
stator/rotor turns ratio, m	3
Stator resistance, R_s	0.001518 Ω
Rotor resistance (referred to stator), R_r	0.002087 Ω
Stator self-inductance, l_s	0.059906 mH
Rotor self-inductance (referred to stator), l_r	0.082060 mH
Mutual inductance, L_m	2.4 mH
Pole pairs, p	2
Angular frequency, ω_s	314.5 rad/s
Synchronous rotor speed, Ω_r	1500 r/min
DC-link voltage, v_{dc}	1200 V

TABLE II
PARAMETERS VALUES OF THE 2-KW DFIG

Rated power	2 kW
Stator voltage	415 V
stator/rotor turns ratio, m	3
Stator resistance, R_s	2.46 Ω
Rotor resistance (referred to stator), R_r	1.767 Ω
Stator self-inductance, l_s	20 mH
Rotor self-inductance (referred to stator), l_r	20 mH
Mutual inductance, L_m	325 mH
Pole pairs, p	2
Angular frequency, ω_s	314.5 rad/s
Synchronous rotor speed, Ω_r	1500 r/min
DC-link voltage, v_{dc}	720 V

REFERENCES

[1] F. Blaabjerg, R. Teodorescu, M. Liserre, and A. Timbus, "Overview of control and grid synchronization for distributed power generation systems," *IEEE Trans. Ind. Electron.*, vol. 53, no. 5, pp. 1398–1409, Oct. 2006.

[2] S. Li, T. Haskew, K. Williams, and R. P. Swatloski, "Control of DFIG wind turbine with direct-current vector control configuration," *IEEE Trans. Sustain. Energy*, vol. 3, no. 1, pp. 1–11, Jan. 2012.

[3] A. M. Howlader, N. Urasaki, and A. Y. Saber, "Control strategies for wind-farm-based smart grid system," *IEEE Trans. Ind. Appl.*, vol. 50, no. 5, pp. 3591–3601, Sep./Oct. 2014.

[4] C. Liu, F. Blaabjerg, W. Chen, and D. Xu, "Stator current harmonic control with resonant controller for doubly fed induction generator," *IEEE Trans. Power Electron.*, vol. 27, no. 7, pp. 3207–3220, Jul. 2012.

[5] L. Xu, D. Zhi, and B. W. Williams, "Predictive current control of doubly fed induction generators," *IEEE Trans. Ind. Electron.*, vol. 56, no. 10, pp. 4143–4153, Oct. 2009.

[6] B. Beltran, M. El Hachemi Benbouzid, and T. Ahmed-Ali, "Second-order sliding mode control of a doubly fed induction generator driven wind turbine," *IEEE Trans. Energy Convers.*, vol. 27, no. 2, pp. 261–269, Jun. 2012.

[7] R. Pena, J. Clare, and G. Asher, "Doubly fed induction generator using back-to-back PWM converters and its application to variable-speed wind-energy generation," *IEE Proc. Electric Power Appl.*, vol. 143, no. 3, pp. 231–241, May 1996.

[8] I. Takahashi and T. Noguchi, "A new quick-response and high-efficiency control strategy of an induction motor," *IEEE Trans. Ind. Appl.*, vol. IA-22, no. 5, pp. 820–827, Sep. 1986.

[9] J. Arbi, M. J.-B. Ghorbal, I. Slama-Belkhodja, and L. Charaa, "Direct virtual torque control for doubly fed induction generator grid connection," *IEEE Trans. Ind. Electron.*, vol. 56, no. 10, pp. 4163–4173, Oct. 2009.

[10] N. R. N. Idris and A. H. M. Yatim, "Direct torque control of induction machines with constant switching frequency and reduced torque ripple," *IEEE Trans. Ind. Electron.*, vol. 51, no. 4, pp. 758–767, Aug. 2004.

[11] G. Abad, M. Á. Rodríguez, and J. Poza, "Two-level VSC based predictive direct torque control of the doubly fed induction machine with reduced torque and flux ripples at low constant switching frequency," *IEEE Trans. Power Electron.*, vol. 23, no. 3, pp. 1050–1061, May 2008.

[12] L. Xu and P. Cartwright, "Direct active and reactive power control of DFIG for wind energy generation," *IEEE Trans. Energy Convers.*, vol. 21, no. 3, pp. 750–758, Sep. 2006.

[13] J. Hu, H. Nian, B. Hu, Y. He, and Z. Zhu, "Direct active and reactive power regulation of DFIG using sliding-mode control approach," *IEEE Trans. Energy Convers.*, vol. 25, no. 4, pp. 1028–1039, Dec. 2010.

[14] H. Nian and Y. Song, "Direct power control of doubly fed induction generator under distorted grid voltage," *IEEE Trans. power Electron.*, vol. 29, no. 2, pp. 894–905, Feb. 2014.

[15] M. K. Bourdoulis and A. T. Alexandridis, "Direct power control of DFIG wind systems based on nonlinear modeling and analysis," *IEEE J. Emerg. Sel. Topics Power Electron.*, vol. 2, no. 4, pp. 764–775, Dec. 2014.

[16] N. Amiri, S. M. Madani, T. Lipo, and H. A. Zarchi, "An improved direct decoupled power control of doubly fed induction machine without rotor position sensor and with robustness to parameter variation," *IEEE Trans. Energy Convers.*, vol. 27, no. 4, pp. 873–884, Dec. 2012.

[17] J. Mohammadi, S. Vaez-Zadeh, S. Afsharnia, and E. Daryabeigi, "A combined vector and direct power control for DFIG-based wind turbines," *IEEE Trans. Sustain. Energy*, vol. 5, no. 3, pp. 767–775, Jul. 2014.

[18] R. Cárdenas, R. Peña, S. Alepuz, and G. Asher, "Overview of control systems for the operation of DFIGs in wind energy applications," *IEEE Trans. Ind. Electron.*, vol. 7, no. 60, pp. 2776–2798, Jul. 2013.

[19] J. Hu, J. Zhu, and D. Dorrell, "Predictive direct power control of doubly fed induction generators under unbalanced grid voltage conditions for power quality improvement," *IEEE Trans. Sustain. Energy*, vol. 6, no. 3, pp. 943–950, Jul. 2015.

[20] A. J. S. Filho and E. R. Filho, "Model-based predictive control applied to the doubly-fed induction generator direct power control," *IEEE Trans. Sustain. Energy*, vol. 3, no. 3, pp. 398–406, Jul. 2012.

[21] E. Rezaei, A. Tabesh, and M. Ebrahimi, "Dynamic model and control of DFIG wind energy systems based on power transfer matrix," *IEEE Trans. Power Del.*, vol. 27, no. 3, pp. 1485–1493, Jul. 2012.

[22] X. Liu and X. Kong, "Nonlinear model predictive control for DFIG-based wind power generation," *IEEE Trans. Autom. Sci. Eng.*, vol. 11, no. 4, pp. 1046–1055, Oct. 2014.

[23] P. Xiong and D. Sun, "Backstepping-based DPC strategy of a wind turbine-driven DFIG under normal and harmonic grid voltage," *IEEE Trans. Power Electron.*, vol. 31, no. 6, pp. 4216–4225, Jun. 2016.

[24] D. Zhi, L. Xu, and B. W. Williams, "Model-based predictive direct power control of doubly fed induction generators," *IEEE Trans. Power Electron.*, vol. 25, no. 2, pp. 341–351, Feb. 2010.

[25] Y. Zhang, J. Hu, and J. Zhu, "Three-vectors-based predictive direct power control of the doubly fed induction generator for wind energy applications," *IEEE Trans. Power Electron.*, vol. 29, no. 7, pp. 3485–3500, Jul. 2014.

[26] W.-H. Chen, D. J. Ballance, P. J. Gawthrop, J. J. Gribble, and J. O'Reilly, "Nonlinear PID predictive controller," *IEE Proc. Control Theory Appl.*, vol. 146, no. 6, pp. 603–611, Nov. 1999.

[27] P. Gawthrop, H. Demircioglu, and I. Siller-Alcala, "Multivariable continuous-time generalised predictive control: A state-space approach to linear and nonlinear systems," *IEE Proc. Control Theory Appl.*, vol. 145, no. 3, pp. 241–250, May 1998.

[28] R. Errouissi, M. Ouhrouche, W.-H. Chen, and A. M. Trzynadlowski, "Robust nonlinear predictive controller for permanent-magnet synchronous motors with an optimized cost function," *IEEE Trans. Ind. Electron.*, vol. 59, no. 7, pp. 2849–2858, Jul. 2012.

[29] V. Kumar and D. Thukaram, "Accurate steady-state representation of a doubly fed induction machine," *IEEE Trans. Power Electron.*, vol. 30, no. 10, pp. 5370–5375, Oct. 2015.

[30] J. Yang and W. X. Zheng, "Offset-free nonlinear MPC for mismatched disturbance attenuation with application to a static var compensator," *IEEE Trans. Circuits Sys. II, Exp. Briefs*, vol. 61, no. 1, pp. 49–53, Jan. 2014.

[31] J. Yang, W. Zheng, S. Li, B. Wu, and M. Cheng, "Design of a prediction accuracy enhanced continuous-time MPC for disturbed systems via a disturbance observer," *IEEE Trans. Ind. Electron.*, vol. 62, no. 9, pp. 5807–5816, Sep. 2015.

[32] S.-K. Chung, "A phase tracking system for three phase utility interface inverters," *IEEE Trans. Power Electron.*, vol. 15, no. 3, pp. 431–438, May 2000.

[33] A. Petersson, L. Harnefors, and T. Thiringer, "Evaluation of current control methods for wind turbines using doubly-fed induction machines," *IEEE Trans. Power Electron.*, vol. 20, no. 1, pp. 227–235, Jan. 2005.

[34] N. Mohan, *Advanced Electric Drives: Analysis, Control and Modeling Using Simulink*. Minneapolis, MN, USA: Mnpere, 2001.

Rachid Errouissi (M'15) received the B.Sc. degree in electronics from the Faculty of Sciences and Technology of Mohammedia, Mohammedia, Morocco, in 1998; the M.Sc. degree in power electronics from Ecole Mohammadia dâĂŹingnieurs, Rabat, Morocco, in 2001; the double M.Sc. degrees in electrical engineering and in automation and system engineering from University Claude Bernard, Lyon, France, in 2002 and 2004, respectively; and the Ph.D. degree in electrical engineering from the University of Quebec, Chicoutimi, QC, Canada, in 2010.

From 2011 to 2014, he was a Postdoctoral Researcher with the Department of Electrical and Computer Engineering, University of New Brunswick. Since 2014, he has been with the Petroleum Institute, Abu Dhabi, UAE, where he is currently conducting research works in renewable energy and advanced control systems. His area of interests include advanced control, nonlinear control, electric machines and drives, and renewable energy conversion systems.

Dr. Errouissi is a Registered Professional Engineer in the province of New Brunswick, Canada.

Ahmed Al-Durra (S'07–M'10–SM'14) received the B.S., M.S., and Ph.D. degrees in electrical and computer engineering from the Ohio State University, Columbus, OH, USA, in 2005, 2007, and 2010, respectively. For his M.Sc. degree, he investigated the application of several nonlinear control techniques on automotive traction PEM fuel cell systems. He conducted his Ph.D. research at the Center for Automotive Research in the Ohio State University on the applications of modern estimation and control theories to automotive propulsion systems.

He is currently an Associate Professor in the Electrical Engineering Department at the Petroleum Institute, Abu Dhabi, UAE. His research interests include application of estimation and control theory in power system stability, micro and smart grids, renewable energy, and process control. He has published more than 70 scientific articles in journals and international conferences.

Dr. Ahmed has successfully accomplished several research projects at international and national levels. He is the Cofounder of the Renewable Energy Laboratory at the Petroleum Institute.

S. M. Muyeen (S'03–M'08–SM'12) received the B.Sc. Eng. degree from the Rajshahi University of Engineering and Technology, Rajshahi, Bangladesh, formerly known as the Rajshahi Institute of Technology, in 2000, and the M.Sc. Eng. and Dr. Eng. degrees from the Kitami Institute of Technology, Kitami, Japan, in 2005 and 2008, respectively, all in system engineering electrical and electronic engineering. His Ph.D. research work focused on wind farm stabilization from the viewpoint of LVRT and frequency fluctuation.

After completing his Ph.D. program, he was a Postdoctoral Research Fellow under the versatile banner of Japan Society for the Promotion of Science from 2008 to 2010 at the Kitami Institute of Technology. He is currently an Associate Professor at the Electrical Engineering Department, Petroleum Institute, Abu Dhabi, UAE. His research interests include power system stability and control, electrical machine, FACTS, energy storage system, renewable energy, and HVdc system. He has been a Keynote Speaker and an Invited Speaker at many international conferences, workshops, and universities. He has published more than 150 articles in different journals and international conferences. He has published five books as an Author or Editor.

Siyu Leng (S'09–M'14) received the B.Sc. degree from Tongji University, Shanghai, China, in 2006. He was granted a full scholarship from Florida State University, Tallahassee, FL, USA, and received the Ph.D. degree in 2012.

During his Ph.D. study, he joined the Center for Advanced Power Systems (CAPS) as a Graduate Research Assistant under the supervision of Prof. D. A. Cartes. His research at CAPS was focused on power quality, especially active power filters. After receiving the Ph.D. degree, he went back to China to work as a Research Engineer with the State Grid Electric Power Research Institute. From May 2013, he was a Postdoctoral Fellow with the University of Alberta, under the supervision of Prof. J. Salmon. His research at the University of Alberta was focused on power electronics, especially induction motor drives. He joined the Petroleum Institute as a Research/Teaching Associate in October 2014. His research interests includes renewable energy, power electronics, motor drive, power quality, and power system analysis.

Frede Blaabjerg (S'86–M'88–SM'97–F'03) was with ABB-Scandia, Randers, Denmark, from 1987 to 1988. He received the Ph.D. degree power electronics from Aalborg University, Aalborg, Denmark, in 1992.

At Aalborg University, he became an Assistant Professor in 1992, an Associate Professor in 1996, and a Full Professor of power electronics and drives in 1998. His current research interests include power electronics and its applications such as in wind turbines, PV systems, reliability, harmonics and adjustable speed drives.

Dr. Blaabjerg received 17 IEEE Prize Paper Awards, the IEEE PELS Distinguished Service Award in 2009, the EPE-PEMC Council Award in 2010, the IEEE William E. Newell Power Electronics Award 2014, and the Villum Kann Rasmussen Research Award 2014. He was an Editor-in-Chief of the IEEE TRANSACTIONS ON POWER ELECTRONICS from 2006 to 2012. He is nominated in 2014 and 2015 by Thomson Reuters to be between the most 250 cited researchers in engineering in the world.